

# Diverse facial inpainting guided by exemplars

Wanglong Lu, Hanli Zhao\*, Xianta Jiang, Xiaogang Jin, Min Wang, Jiankai Lyu, and Kaijie Shi

**Abstract**—Facial image inpainting is a task of filling visually realistic and semantically meaningful contents for missing or masked pixels in a face image. Although existing methods have made significant progress in achieving high visual quality, the controllable diversity of facial image inpainting remains an open problem in this field. This paper introduces EXE-GAN, a novel diverse and interactive facial inpainting framework, which can not only preserve the high-quality visual effect of the whole image but also complete the face image with exemplar-like facial attributes. The proposed facial inpainting is achieved based on generative adversarial networks by leveraging the global style of input image, the stochastic style, and the exemplar style of exemplar image. A novel attribute similarity metric is introduced to encourage networks to learn the style of facial attributes from the exemplar in a self-supervised way. To guarantee the natural transition across the boundary of inpainted regions, a novel spatial variant gradient backpropagation technique is designed to adjust the loss gradients based on the spatial location. A variety of experimental results and comparisons on public CelebA-HQ and FFHQ datasets are presented to demonstrate the superiority of the proposed method in terms of both the quality and diversity in facial inpainting.

**Index Terms**—Image editing, image inpainting, facial inpainting, facial attribute transfer, generative adversarial networks.

## I. INTRODUCTION

NOWADAYS, the image has become a common medium for daily communication. As an interesting branch of image inpainting, face image inpainting fills missing or masked regions in face images with realistic visual contents. Compared to inpainting natural scene images like forests and oceans, face image inpainting is more challenging since faces have much stronger topological structure and attribute consistency to preserve. Face inpainting backs a variety of applications, such as portrait retouching, photograph restoration [1], and image extrapolation [2]. Given guidance information, users can easily infer what the missing regions possibly look like. There is an increasing demand even for a novice to generate realistic images as desired with minimum guidance information.

Many inpainting methods [3], [4], [5] have been proposed to generate a single inpainting result for a missing region. However, since image inpainting is an underdetermined inverse problem, usually multiple inpainting solutions satisfy the semantically meaningful requirement of inpainting. Some methods [8], [7], [9] strive to generate multiple diverse image inpainting results and allow users to select a desired result from these outputs. However, these methods still cannot

W. Lu, H. Zhao, M. Wang, J. Lyu, and K. Shi are with the College of Computer Science and Artificial Intelligence, Wenzhou University, Wenzhou, China.

W. Lu and X. Jiang are with the Department of Computer Science, Memorial University of Newfoundland, St. John's, Canada.

X. Jin is with the State Key Lab of CAD&CG, Zhejiang University, Hangzhou, China.

\* Corresponding author. E-mail: hanlizhao@wzu.edu.cn

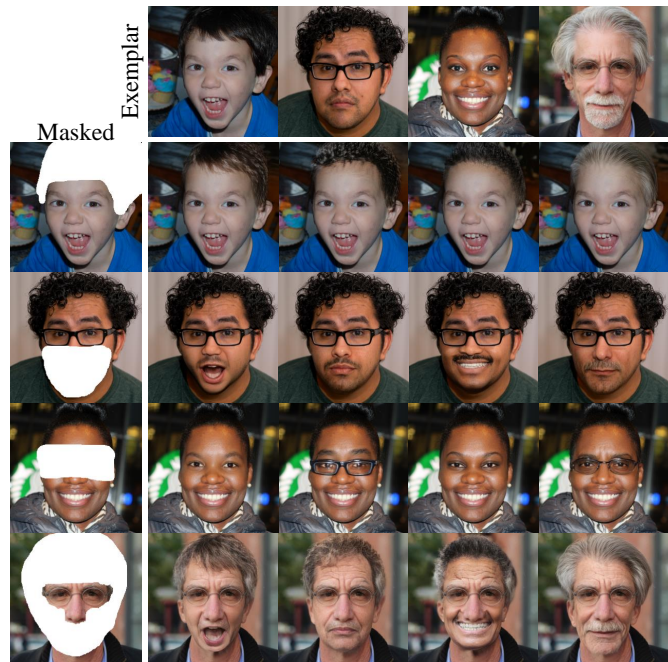


Fig. 1. Examples of our diverse facial inpainting guided by exemplars.

complete missing regions with user preferences. Some recent methods try to employ additional landmarks [10], strokes [11], or sketches [11], [12], [13] to guide the inpainting of facial structures and attributes. However, these methods tend to overfit the resulting images with the limited guidance information and the variety of completed solutions is quite limited. Therefore, these methods usually require considerable professional skills in order to generate satisfied target facial attributes, such as identity, expression, and gender.

Recently, many face manipulation methods have been proposed to achieve impressive performance for the manipulation of facial attributes based on the guidance information, such as geometries [14], [15], semantics [16], [17], and exemplars [18], [19]. However, in addition to manipulated regions, these face manipulation methods involve unwanted changes of colors in unedited regions, which makes these methods not feasible to facial image inpainting since users expect that the visual information of known regions should remain unchanged. This motivates us to explore an efficient facial inpainting method which can generate multiple diverse face images guided by a single exemplar image without changing colors of known regions.

To this end, we propose EXE-GAN, a novel diverse and interactive facial inpainting framework, which enables high-quality facial inpainting guided by exemplars, as shown in

Fig. 1. The proposed framework consists of four main components, including a mapping network, a style encoder, a multi-style generator, and a discriminator. The global style of input image, the stochastic style, and the exemplar style of exemplar image are mixed to generate the completed result. We impose a perceptual loss between deep features of the input image and the completed result to preserve the global visual consistency. In order to enable the completion of exemplar-like facial attributes, we further employ a facial identity loss and an attribute loss between the exemplar and the completed result. A novel spatial variant gradient backpropagation technique is introduced for network training to guarantee the natural transition across the boundary of inpainted regions. Thus, the diversity of our facial inpainting solution is reflected in many aspects, that is, inherent stochasticity, multiple exemplars, style mixing, and code tuning. The proposed method is comprehensively evaluated on public CelebA-HQ [22] and FFHQ [23] datasets. A variety of experimental comparisons show that the proposed method outperforms the state-of-the-art methods in high-quality diverse facial inpainting. The proposed method can not only preserve the global visual consistency of the whole image but also complete the face image with exemplar-like facial attributes.

In summary, this paper has the following contributions:

- A novel diverse facial inpainting framework is proposed for the high-quality inpainting of face image with facial attributes looking like the exemplar image.
- A self-supervised attribute similarity metric is proposed to help the generative network learn the style of facial attributes from the exemplar.
- A novel spatial variant gradient backpropagation technique is introduced for network training to guarantee the realistic inpainting on the boundary.
- A variety of experiments demonstrate the superiority of the proposed method in terms of the diversity and visual quality in facial inpainting.

## II. RELATED WORK

### A. Image inpainting

Traditional image inpainting techniques mainly leverage low-level features to inpaint missing regions. Diffusion-based methods [25], [26], [24] propagate information along the hole boundary to the hole center. These methods can perform well for small and narrow missing regions, but fail to recover meaningful contents for large holes. Patch-based methods [27], [28], [29] search and copy similar patches from image datasets or known image background in an iterative fashion. Recent variants include GPU-based parallel methods [30], [31], summarizing of non-stationary patterns [32], and inpainting with nonlocal texture similarity [33]. Patch-based methods fill missing holes using similar patches but lack of semantic understanding for the image.

Deep-learning-based inpainting methods employ deep neural networks and generative adversarial networks (GANs) [34] to achieve semantic completion. A lot of efforts have been made to improve the visual quality, such as inpainting by

deep neural networks [35], [36], [37], introducing conditional-GANs [38], exploiting both global and local discriminators [3], improving semantic understanding [39], [40], [41], adopting novel loss functions or regularization [4], [42], handling irregular holes [12], [5], designing novel modules or architectures [4], [42], [43], [44], [45], [46], high-resolution inpainting [47], [6], and coarse-to-fine inpainting [48], [49]. These methods aim at semantically high-quality completion but cannot generate multiple diverse results.

Some recent studies try to fulfill the task of diverse image inpainting. UCTGAN [7] achieves the diversity of repaired regions by projecting both the instance image distribution and the conditional completion image space into the low-dimensional manifold space. Co-Mod-GAN [9] succeeds in completing large-scale missing regions and obtains diverse results by introducing inherent stochasticity. Besides, by taking advantage of auxiliary information, such as landmarks [10], sketches [12], [13], [11], and geometries [50], [51], structures and attributes of inpainted regions can be generated accordingly. Since facial attributes contain lots of visual information including color, geometry, texture, and light, these methods tend to overfit with these guidance information. As a result, the variety of completed solutions is quite limited. Different from these methods, the proposed method can effectively generate realistic diverse inpainted face images guided by a single exemplar image.

### B. Facial attribute transfer

Facial attribute transfer can be achieved by face manipulation methods using latent-guided codes or reference images. Semantic-level face manipulation methods can control a set of attributes, e.g., with or without glasses. By using a domain label to index the mapped style codes, StarGANv2 [17] learns the mixed style to translate an image of one domain to diverse images of a target domain. Using hierarchical style disentanglement, Li et al. [19] proposed a translation process for controllable translations of both multi-label and multi-style. Many other semantic-level methods [55], [56], [16] have also been proposed to achieve impressive performance for recent years. However, these methods only operate on a set of pre-defined attributes and leave users little freedom for face manipulation.

Geometry-based face manipulation methods implement exemplar-based facial transfer based on semantic geometry. MaskGAN [14] uses the semantic mask as an intermediate representation for flexible interactive face editing. SEAN [57] employs the segmentation mask to control the style of each semantic region individually. By decoupling portraits' latent space into a geometry space and a texture space, SofGAN [15] implicitly learns 3D geometric information from 2D semantic masks and enables dynamic styling. Since information loss occurs in the projection and reconstruction between real-captured photos and corresponding representations, these methods tend to change fine details for background.

Exemplar-based face manipulation methods transfer facial attributes from exemplars at instance level. ELEGANT [18] transfers facial attributes by exchanging certain parts of

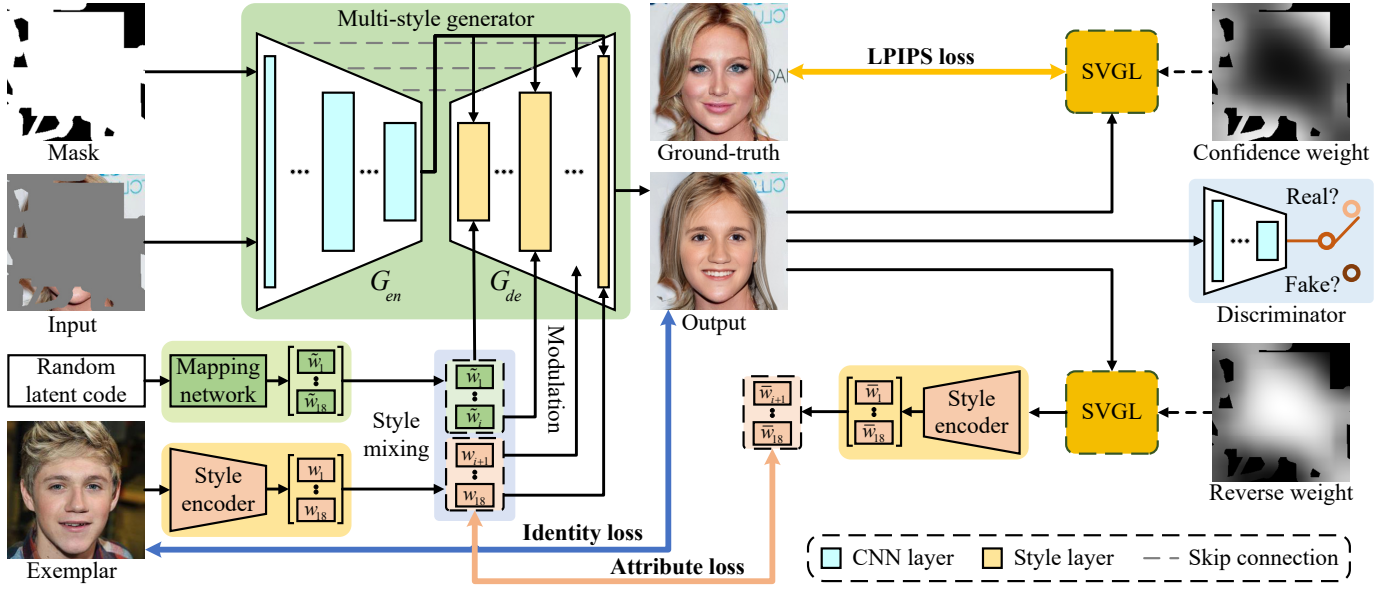


Fig. 2. Overall structure of our EXE-GAN framework. We employ style mixing on stochastic and exemplar style codes, and modulate them with the global style latent code of input image into the multi-style generator for diverse facial inpainting. The adversarial loss, identity loss, LPIPS loss, and attribute loss are combined as a total training objective. Spatial variant gradient layers are utilized for natural transition across the filling boundary.

encodings between faces. MulGAN [52] can balance the quality of generated images and attribute transferring ability. FaceShifter [53] performs high fidelity and occlusion aware face swapping with a two-stage framework. SimSwap [54] extends the identity-specific face swapping to arbitrary face swapping by applying their ID injection module and weak feature matching loss. Nevertheless, these methods have a common drawback that users cannot flexibly select facial regions for local transfer of facial attributes. On the contrary, our method transfers local facial attributes from exemplars interactively while keeping known regions unchanged.

### C. Image embedding

Our work is also closely related to image embedding which enables image synthesis in latent space. StyleGAN [23] and StyleGANv2 [58] enable direct scale-specific control of image synthesis with disentangled intermediate latent style space and can produce excellent results for unconditional face image synthesis. Abdal et al. [59] optimized latent codes in an extended latent space with the concatenation of 18 different 512-dimensional vectors. They further proposed an activation tensor manipulation method [60] to perform flexible image editing in the extended style latent space. Recently, Richardson et al. [62] introduced a residual feature pyramid network as the encoder of their pixel2style2pixel framework to extract the extended latent code from a given image efficiently. Many other methods [61], [63], [64] perform the image modification by inverting an image to the latent space.

Although image embedding has the powerful capability of presenting image styles, it is not trivial for diverse facial inpainting. In our work, we plan to develop a novel method for the completion of facial attributes by taking advantage of latent style codes. We first invert the input and exemplar images to

latent style codes and then feed to the generative network to perform diverse facial inpainting.

## III. METHOD

### A. Overview

As shown in Fig. 2, given a ground-truth face image  $I_{gt} \in \mathbb{R}^{h \times w \times 3}$ , an exemplar image  $I_{exe} \in \mathbb{R}^{h \times w \times 3}$ , and a binary mask  $M \in \mathbb{R}^{h \times w \times 1}$  (with value 1 for unknown and 0 for known pixels), the input image  $I_{in} \in \mathbb{R}^{h \times w \times 3}$  is obtained as  $I_{in} = I_{gt} \odot (1 - M)$ , where  $\odot$  denotes the Hadamard product. The goal of our EXE-GAN framework is to automatically generate a realistic face image  $I_{out}$  where the inpainting of masked regions in  $I_{in}$  is guided by facial attributes of  $I_{exe}$  while known regions remaining unchanged. The proposed EXE-GAN consists of four main components, including a mapping network, a style encoder, a multi-style generator, and a discriminator.

1) *Mapping network*: A multi-layer fully-connected neural network  $f$  [58], [9] linearly maps a randomly sampled latent code  $z \in \mathbb{R}^{512 \times 1}$  to a stochastic style code  $\tilde{w} = \{\tilde{w}_i \in \mathbb{R}^{512 \times 1} | i \in T\} \in \tilde{W}+$ , where  $\tilde{W}+$  denotes extended stochastic style latent space and  $T = \{1, 2, \dots, 18\}$  denotes the index set. Let  $\theta_f$  be the learnable network parameters in  $f$ , we have  $\tilde{w} = f(z; \theta_f)$ .

2) *Style encoder*: A pre-trained pixel2style2pixel style encoder  $E$  [62], [63] directly maps an image to a disentangled style latent space  $W+$ . Given the pre-trained network parameters  $\hat{\theta}_e$ , the style encoder is used to obtain the exemplar style code  $w = \{w_i \in \mathbb{R}^{512 \times 1} | i \in T\} = E(I_{exe}; \hat{\theta}_e) \in W+$  and the inpainted style code  $\bar{w} = \{\bar{w}_i \in \mathbb{R}^{512 \times 1} | i \in T\} = E(I_{out}; \hat{\theta}_e) \in W+$ .

3) *Multi-style generator*: A generative network  $G$  that leverages multiple representations (i.e.,  $I_{in}$ ,  $M$ , and  $\hat{w}$ ) to generate the intermediate inpainting  $I_{pred} \in \mathbb{R}^{h \times w \times 3}$ , where  $\hat{w} = \{\hat{w}_i \in \mathbb{R}^{512 \times 1} | i \in T\}$  is the mixed style code of  $w$  and  $\tilde{w}$ . Let  $\theta_g$  be learnable network parameters of  $G$ , we have  $I_{pred} = G(I_{in}, M, \hat{w}; \theta_g, \theta_f)$ . The multi-style generator can be further divided into an encoder  $G_{en}$  and a decoder  $G_{de}$ , that is,  $G = \{G_{en}, G_{de}\}$ .

4) *Discriminator*: A discriminative network  $D$  as in [58], [9] that learns to judge whether an image is a real or fake image. Let  $\theta_d$  be learnable network parameters of  $D$ , the discriminative network maps the inpainted image  $I_{out}$  to a scalar  $D(I_{out}; \theta_d) \in \mathbb{R}^{1 \times 1}$ .

### B. Multi-style modulation

To leverage the global style of input image, the stochastic style, and the exemplar style of exemplar image to perform diverse facial inpainting, we build upon the generator of Comod-GAN [9] and extend it to our multi-style generator  $G$ . The proposed multi-style generator can not only preserve the global visual consistency of input image, but also embed exemplar facial attributes to the local facial inpainting. In addition, it has the good property of inherent stochasticity with the stochastic style latent code.

First of all, the mixed style code  $\hat{w}$  is obtained by style mixing [23], [58]. Specifically, each channel of  $\hat{w}$  is defined as:

$$\hat{w}_i = \begin{cases} w_i & \text{if } \phi_i = 1, \\ \tilde{w}_i & \text{otherwise,} \end{cases} \quad (1)$$

where  $i \in T = \{1, 2, \dots, 18\}$  and  $\phi \in \mathbb{R}^{18 \times 1}$  is a binary vector to indicate which style is modulated for each channel. Unless specified, we set  $\phi = [0, 0, 0, 0, 0, 1, 1, \dots, 1]$  in this paper.

Secondly, the encoder  $G_{en}$  takes  $I_{in}$  and  $M$  as input, and outputs a global style code  $c \in \mathbb{R}^{2 \times 512 \times 1}$  as well as corresponding multi-resolution feature maps.

Then, as illustrated in Fig. 2, the global style code  $c$  and the mixed style code  $\hat{w}$  are transformed to multi-style vectors  $v$  for subsequent modulation within style layers of the decoder  $G_{de}$ . For each  $i^{th}$  style layer, the transformation is defined as [58]:

$$v_i = \mathcal{A}_i(c, \hat{w}_i), \quad (2)$$

where  $\mathcal{A}_i$  is a learned affine transformation within  $i^{th}$  style layer and  $v_i$  is a linearly learned style representation conditioning on the input style representations.

Next, the decoder  $G_{de}$  utilizes the multi-style vectors  $v$  and the multi-resolution feature maps output by  $G_{de}$  to generate the intermediate inpainting  $I_{pred}$ . The decoder contains two style layers in each resolution. In each  $i^{th}$  style layer, the multi-style vector  $v_i$  is then used for weight modulation and demodulation [58], [9]. As shown in Fig. 2, skip connections are used for collecting the multi-resolution feature maps in the decoder  $G_{de}$ .

Finally, the inpainted image  $I_{out}$  is generated as follows:

$$I_{out} = I_{in} \odot (1 - M) + I_{pred} \odot M. \quad (3)$$

### C. Training objectives

Our framework is trained to optimize the learnable network parameters  $\theta_g$ ,  $\theta_f$ , and  $\theta_d$  using the following objectives.

1) *Adversarial loss*: We use the adversarial non-saturating logistic loss [34] with  $R_1$  regularization [65]. Specifically, the adversarial objective is defined as:

$$\begin{aligned} \mathcal{L}_{adv}(I_{out}, I_{gt}) = & \mathbb{E}_{I_{out}}[\log(1 - D(I_{out}))] \\ & + \mathbb{E}_{I_{gt}}[\log(D(I_{gt}))] - \frac{\gamma}{2} \mathbb{E}_{I_{gt}}[\|\nabla_{I_{gt}} D(I_{gt})\|_2^2], \end{aligned} \quad (4)$$

where  $\gamma$  is used to balance the  $R_1$  regularization term. We set  $\gamma = 10$  in this paper.

The generative network  $G$  learns to generate a visually realistic image  $I_{out}$  while the discriminative network  $D$  tries to distinguish between the ground-truth  $I_{gt}$  and the generated one  $I_{out}$ .  $G$  and  $D$  are trained in an alternating manner.

2) *Identity loss*: We constrain identity similarity between the output image  $I_{out}$  and the exemplar image  $I_{exe}$  in the embedding space. The identity loss is formulated as follows:

$$\mathcal{L}_{id}(I_{out}, I_{exe}) = 1 - \cos(R(I_{out}), R(I_{exe})), \quad (5)$$

where  $R(\cdot)$  is a pre-trained ArcFace network [66] for face recognition.

3) *LPIPS loss*: As demonstrated in [69], the Learned Perceptual Image Patch Similarity (LPIPS) metric [21] keeps better image quality compared to the standard perceptual loss [68]. We employ the LPIPS loss to constrain the perceptual similarity between the output image  $I_{out}$  and the ground-truth  $I_{gt}$ :

$$\mathcal{L}_{lpiPs}(I_{out}, I_{gt}) = \begin{cases} \|F(I_{out}) - F(I_{gt})\|_2 & \text{if } I_{gt} = I_{exe} \\ 0 & \text{otherwise} \end{cases}, \quad (6)$$

where  $F(\cdot)$  is the pre-trained perceptual feature extractor and we adopt VGG [70] in our work. Note that  $\mathcal{L}_{lpiPs}$  is applied only when  $I_{gt}$  and  $I_{exe}$  are sampled from the same image.

4) *Attribute loss*: In order to learn the style of facial attributes from the exemplar image, we proposed a novel self-supervised attribute consistency metric to measure the similarity between facial attributes of the inpainted result  $I_{out}$  and the exemplar  $I_{exe}$  in the latent style space:

$$\mathcal{L}_{attr}(I_{out}, I_{exe}) = \frac{1}{\|\phi\|_1} \sum_{i \in T} \phi_i \cdot \|\bar{w}_i - \hat{w}_i\|_2, \quad (7)$$

where  $\|\cdot\|_1$  is L1 norm which indicates the number of non-zeros.

5) *Total objective*: After defining loss functions above, the total training objective can be expressed as:

$$\begin{aligned} O(\theta_g, \theta_f, \theta_d, \hat{\theta}_e) = & \mathcal{L}_{adv}(I_{out}, I_{gt}) + \lambda_{id} \mathcal{L}_{id}(I_{out}, I_{exe}) \\ & + \lambda_{lpiPs} \mathcal{L}_{lpiPs}(I_{out}, I_{gt}) + \lambda_{attr} \mathcal{L}_{attr}(I_{out}, I_{exe}), \end{aligned} \quad (8)$$

where  $\lambda_{id}$ ,  $\lambda_{lpiPs}$ , and  $\lambda_{attr}$  are weights of corresponding losses, respectively. We set  $\lambda_{id} = 0.1$ ,  $\lambda_{attr} = 0.1$ , and  $\lambda_{lpiPs} = 0.5$  in this paper.

During training, we can obtain the optimized parameters  $\theta_g$ ,  $\theta_f$ , and  $\theta_d$  via the minimax game iteratively:

$$\begin{aligned} (\theta_g, \theta_f) = & \arg \min_{\theta_g, \theta_f} O(\theta_g, \theta_f, \theta_d, \hat{\theta}_e), \\ (\theta_d) = & \arg \max_{\theta_d} O(\theta_g, \theta_f, \theta_d, \hat{\theta}_e). \end{aligned} \quad (9)$$

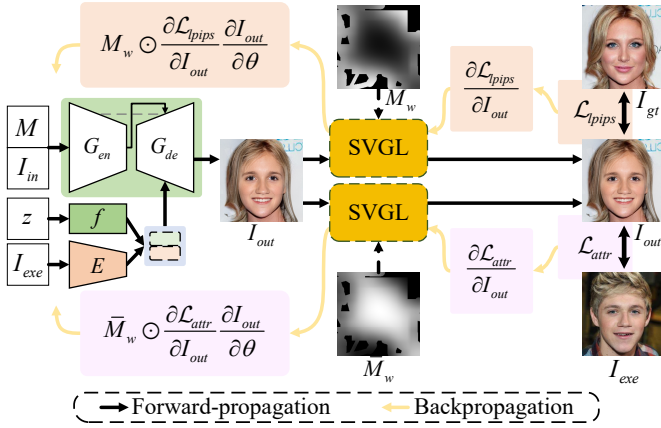


Fig. 3. Illustration of the SVGL on LPIPS and attribute losses. In forward-propagation, SVGL does not change any information for  $I_{out}$ . In backpropagation, gradients are re-weighted based on the spatial variant  $M_w$  and  $\bar{M}_w$ , respectively.

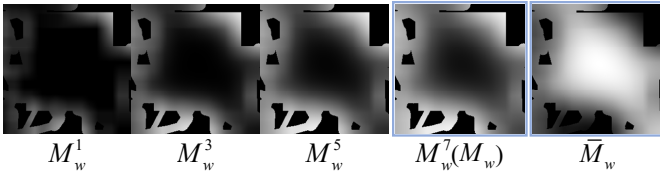


Fig. 4. Visualization of the evolution of confidence weight mask  $M_w$  with 1, 3, 5, and 7 iterations, respectively.

#### D. Spatial variant gradient backpropagation

It is expected that the inpainted facial attributes close to the filling center are more similar to those of exemplar image. Moreover, the inpainted values close to the filling boundary should be perceptually more similar to those of input image and visual contents should be naturally transitioned on the boundary. Therefore, in order to generate naturally looking inpainting, we further exerted constraint based on spatial location.

From Eq. 6 and Eq. 7, we can find that the LPIPS loss and attribute loss are defined over the entire inpainted image. GMCNN [4] applies the spatial constraint to the pixel-wise reconstruction loss. However, we cannot directly impose GMCNN’s spatial constraint on our loss functions. The reason is that our losses are defined in embedding space and dimensions of embedding features do not match those of the spatial space. Therefore, a more sophisticated scheme should be designed with the spatial constraint.

1) *Spatial variant gradient layer*: Inspired by the studies of domain adaptation [72] and network fine-tuning [73] which manipulate gradients in backpropagation, we designed a novel spatial variant gradient layer (SVGL) to impose the spatial constraint on loss gradients in backpropagation.

As shown in Fig. 3, SVGL has no parameter but relies on a spatial weight mask. During forward-propagation, it acts as an identity transform, which does not change any information from input. During backpropagation, SVGL collects gradients

#### Algorithm 1 Training procedure of EXE-GAN

- 1: **while**  $f$ ,  $G$ , and  $D$  have not converged **do**
- 2:   Sample batch images  $\mathcal{I}_{gt}$  from training data
- 3:   Sample random latent vectors  $\mathcal{Z}$
- 4:   Sample a random number  $r \in [0, 1]$
- 5:   **if**  $r < \text{threshold } \tau$  **then**
- 6:     Sample batch exemplars  $\mathcal{I}_{exe}$  from training data
- 7:   **else**
- 8:     Set batch exemplars from ground-truth  $\mathcal{I}_{exe} \leftarrow \mathcal{I}_{gt}$
- 9:   Create random masks  $\mathcal{M}$  for  $\mathcal{I}_{in}$
- 10:   Get confidence weight masks  $M_w$  for  $\mathcal{L}_{lpiPS}$
- 11:   Get reverse weight masks  $\bar{M}_w$  for  $\mathcal{L}_{attr}$
- 12:   Get inputs  $\mathcal{I}_{in} \leftarrow \mathcal{I}_{gt} \odot (1 - \mathcal{M})$
- 13:   Get  $\mathcal{I}_{pred} \leftarrow G(\mathcal{I}_{in}, \mathcal{M}, \text{mixing}(E(\mathcal{I}_{exe}), f(\mathcal{Z})))$
- 14:   Get outputs  $\mathcal{I}_{out} \leftarrow \mathcal{I}_{in} \odot (1 - \mathcal{M}) + \mathcal{I}_{pred} \odot \mathcal{M}$
- 15:   Update  $f$  and  $G$  with  $\mathcal{L}_{adv}$ ,  $\mathcal{L}_{id}$ ,  $\mathcal{L}_{lpiPS}$ , and  $\mathcal{L}_{attr}$
- 16:   Update  $D$  with  $\mathcal{L}_{adv}$

from subsequent layers, re-weights these gradients based on the spatial weight mask, and passes the re-weighted gradients to preceding layers.

Mathematically, given an input feature  $x$  and a spatial weight mask  $M_x$  with the same size as  $x$ , we can treat SVGL as a “pseudo-function”  $P(x, M_x)$ . The forward-propagation and backpropagation behaviors of SVGL are defined below:

$$\begin{aligned} P(x, M_x) &= x, \\ \frac{\partial P(x, M_x)}{\partial x} &= M_x \odot \mathbf{I}, \end{aligned} \quad (10)$$

where  $\mathbf{I}$  represents an identity matrix.

2) *Spatial variant optimization using SVGL*: Here we present how to apply SVGL to the spatial variant LPIPS loss and the spatial variant attribute loss to improve the quality of the inpainted image. Note that our novel SVGL is general and can be used to apply spatial constraints to any loss functions with spatial variant backpropagation.

We generated a confidence weight mask  $M_w \in \mathbb{R}^{h \times w \times 1}$  where pixels close to the filling boundary are more constrained than those away from the boundary. Following GMCNN [4], this was achieved by iteratively applying a Gaussian filter  $g$  to the inpainting mask  $M$ :

$$M_w^i = (g \otimes (1 - M + M_w^{i-1})) \odot M, \quad (11)$$

where the size of  $g$  is  $64 \times 64$  with standard deviation of 40,  $\otimes$  denotes the convolutional operator, and  $M_w^0 = 0$ . By repeating Eq. 11 several times, we obtained the confidence weight mask  $M_w = M_w^t$ , where  $t = 7$  in this paper.

Then, we created a reverse weight mask  $\bar{M}_w \in \mathbb{R}^{h \times w \times 1}$  from the confidence weight mask  $M_w$  as follows:

$$\bar{M}_w = (1 - M_w) \odot M. \quad (12)$$

The evolution of confidence weight mask is as illustrated in Fig. 4.

Next, we equipped the network with a SVGL  $P(\cdot, M_w)$  for the spatial variant LPIPS loss and a SVGL  $P(\cdot, \bar{M}_w)$  for the spatial variant attribute loss. As shown in Fig. 3, both SVGLs were added right after the layer of generating  $I_{out}$ .

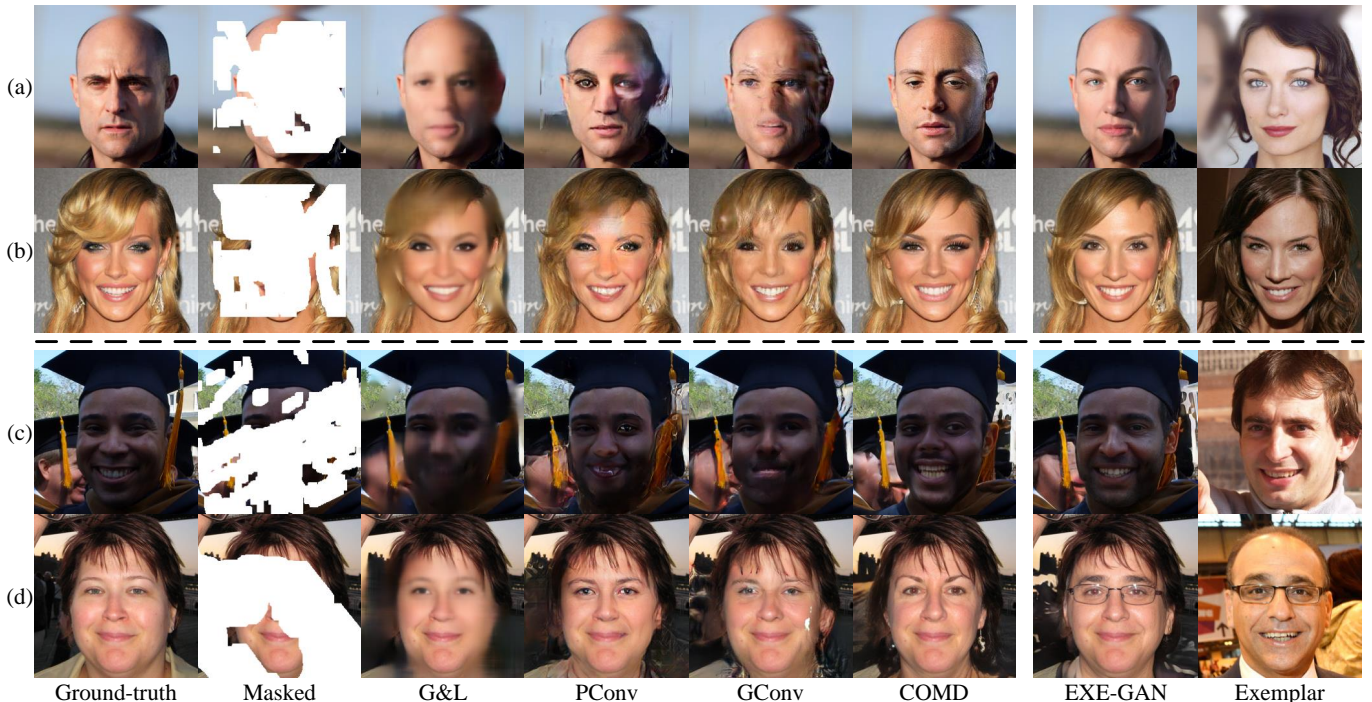


Fig. 5. Qualitative comparison of our method with state-of-the-art free-form inpainting methods on (a-b) CelebA-HQ and (c-d) FFHQ datasets.

With the spatial variant gradient layers, the training objective was computed with Eq. 8 during forward-propagation but its gradients were computed in a spatial variant manner. Therefore, the proposed spatial variant LPIPS loss effectively focuses on the learning of perceptual similarity of the filling boundary while the proposed spatial variant attribute loss learns the style similarity between facial attributes of the filling center and the exemplar image.

The pseudo-code of the training procedure of our EXE-GAN framework is provided in Algorithm 1. The threshold  $\tau \in [0, 1]$  was used to control the probability that the sampled raw image  $I_{gt}$  and exemplar image  $I_{exe}$  were the same. We set threshold  $\tau = 0.9$  in this paper.

## IV. EXPERIMENTS

### A. Settings

1) *Datasets*: Experiments were conducted on two publicly available face image datasets below:

- CelebA-HQ [22]: A high-quality image dataset that consists of 30,000 portrait images extracted from the CelebA dataset [74]. We randomly selected 2,8000 images for training and remaining 2000 images for testing. Each image was resized to the size of  $256 \times 256$ .
- FFHQ [23]: A high-quality image dataset with more variations, consisting of 70,000 face images [23]. We randomly selected 60,000 images for training and the rest images for testing. Each image was resized to the size of  $256 \times 256$ .

2) *Evaluation metrics*: The performance was quantitatively evaluated using the metrics below:

- Fréchet inception distance (FID) [75]: A measure for the visual quality of generated images. FID has been proven to correlate well with human perception.
- Paired/unpaired inception discriminative score (P-IDS/U-IDS) [9]: A recently proposed robust assessment for the perceptual fidelity of generative models.

3) *Implementation details*: The proposed EXE-GAN framework was implemented using Python and PyTorch. Following the settings of StyleGANv2 [58] and Co-modGAN [9], we employed the Adam optimizer with the first momentum coefficient  $\beta_1 = 0.5$ , the second momentum coefficient  $\beta_2 = 0.99$ , and the learning rate of 0.002. Mixing regularization [23] with a probability of 0.5 was employed to generate stochastic style codes during training. The free-form mask sampling strategy was adopted for training by simulating random brush strokes and rectangles. The brush strokes were generated using the algorithm presented in GConv [12] with maxVertex of 20, maxLength of 100, maxBrushWidth of 24, maxAngle of 360. The multiple rectangles were generated where the number of up-to-half-size rectangles was uniformly sampled within  $[0, 5]$  and the number of up-to-quarter-size rectangles was uniformly sampled within  $[0, 10]$ . We trained the networks for 800,000 iterations with the batch size of 8. All experiments were conducted on the NVIDIA Tesla V100 GPU. The training time was around three weeks.

TABLE I  
QUANTITATIVE COMPARISON OF OUR METHOD WITH THE STATE-OF-THE-ART FREE-FORM INPAINTING METHODS ON THE CELEBA-HQ DATASET.  $\uparrow$  HIGHER IS BETTER.  $\downarrow$  LOWER IS BETTER. **BOLD**: TOP-2 QUANTITY.

Metric	Mask	G&L [3]	CA [40]	PConv [5]	GConv [12]	RN [46]	EdgeConnect [13]	GMCNN [4]	CMOD [9]	Ours
FID $\downarrow$	10-20%	5.262	4.699	10.00	3.460	32.88	3.959	4.474	<b>2.352</b>	<b>2.312</b>
	20-30%	10.62	8.232	9.441	5.451	25.56	6.763	6.630	<b>3.793</b>	<b>3.667</b>
	30-40%	17.02	12.36	10.16	7.116	19.36	9.841	9.672	<b>5.214</b>	<b>5.125</b>
	40-50%	23.76	17.50	12.51	9.521	18.97	14.07	12.60	<b>6.817</b>	<b>6.700</b>
	50-60%	30.22	25.81	16.60	13.61	36.97	22.51	18.75	<b>8.643</b>	<b>8.657</b>
	Fixed	11.15	7.116	6.231	<b>4.459</b>	12.49	9.528	7.461	4.985	<b>4.750</b>
U-IDS $\uparrow$	10-20%	2.375%	3.05%	2.250%	13.52%	0	12.10%	9.199%	<b>26.82%</b>	<b>25.90%</b>
	20-30%	0	0.05%	0.300%	5.75%	0	2.375%	3.474%	<b>23.32%</b>	<b>22.15%</b>
	30-40%	0	0	0	0.85%	0	0.20%	0.024%	<b>19.72%</b>	<b>20.40%</b>
	40-50%	0	0	0	0.050%	0	0	0	<b>16.92%</b>	<b>16.18%</b>
	50-60%	0	0	0	0	0	0	0	<b>11.35%</b>	<b>10.95%</b>
	Fixed	0	0.025%	0.95%	7.200%	0	0	0.30%	<b>12.02%</b>	<b>13.12%</b>
P-IDS $\uparrow$	10-20%	0.50%	0.30%	0.550%	5.65%	0	3.30%	2.20%	<b>17.70%</b>	<b>15.15%</b>
	20-30%	0	0.05%	0.05%	1.25%	0	0.15%	0.25%	<b>13.80%</b>	<b>12.40%</b>
	30-40%	0	0	0	0.15%	0	0	0	<b>9.60%</b>	<b>10.30%</b>
	40-50%	0	0	0	0	0	0	0	<b>7.60%</b>	<b>8.20%</b>
	50-60%	0	0	0	0	0	0	0	<b>4.35%</b>	<b>4.15%</b>
	Fixed	0	0	0.15%	2.300%	0	0	0	<b>5.40%</b>	<b>5.80%</b>

TABLE II  
QUANTITATIVE COMPARISON OF OUR METHOD WITH THE STATE-OF-THE-ART FREE-FORM INPAINTING METHODS ON THE FFHQ DATASET.  $\uparrow$  HIGHER IS BETTER.  $\downarrow$  LOWER IS BETTER. **BOLD**: TOP-2 QUANTITY.

Metric	Mask	G&L [3]	CA [40]	PConv [5]	GConv [12]	RN [46]	EdgeConnect [13]	GMCNN [4]	CMOD [9]	Ours
FID $\downarrow$	10-20%	3.262	2.463	9.840	2.097	15.26	1.681	1.811	<b>0.822</b>	<b>0.771</b>
	20-30%	7.673	5.523	7.948	3.075	14.88	3.330	3.451	<b>1.412</b>	<b>1.324</b>
	30-40%	13.05	9.697	6.874	4.730	16.07	5.830	5.455	<b>2.016</b>	<b>1.953</b>
	40-50%	19.47	15.06	8.504	7.189	20.48	10.43	8.534	<b>2.696</b>	<b>2.641</b>
	50-60%	27.36	23.49	10.92	11.42	36.05	25.75	15.56	<b>3.756</b>	<b>3.824</b>
	Fixed	6.452	4.188	4.352	<b>1.915</b>	5.496	7.920	4.680	<b>2.189</b>	2.321
U-IDS $\uparrow$	10-20%	17.40%	19.585%	19.07%	26.22%	3.350%	27.89%	27.67%	<b>38.96%</b>	<b>39.22%</b>
	20-30%	6.485%	8.205%	15.01%	19.48%	1.237%	18.56%	18.09%	<b>34.02%</b>	<b>34.28%</b>
	30-40%	0.485%	1.595%	11.18%	13.13%	0.008%	10.93%	12.23%	<b>30.55%</b>	<b>30.01%</b>
	40-50%	0	0	7.20%	8.05%	0	4.910%	6.50%	<b>26.17%</b>	<b>26.35%</b>
	50-60%	0	0	3.635%	3.68%	0	0.014%	0.465%	<b>23.03%</b>	<b>23.60%</b>
	Fixed	6.84%	9.795%	13.17%	26.07%	9.704%	8.415%	10.89%	<b>28.37%</b>	<b>28.41%</b>
P-IDS $\uparrow$	10-20%	0.58%	0.93%	2.86%	3.77%	0.050%	3.370%	2.570%	<b>15.13%</b>	<b>15.05%</b>
	20-30%	0.08%	0.09%	1.09%	1.53%	0	0.95%	0.63%	<b>11.17%</b>	<b>11.47%</b>
	30-40%	0.01%	0.01%	0.53%	0.60%	0	0.36%	0.29%	<b>9.67%</b>	<b>9.89%</b>
	40-50%	0	0	0.22%	0.36%	0	0.06%	0.07%	<b>7.89%</b>	<b>8.31%</b>
	50-60%	0	0	0.10%	0.05%	0	0	0	<b>7.66%</b>	<b>7.68%</b>
	Fixed	0.09%	0.190%	0.72%	6.47%	0.24%	0.23%	0.21%	<b>10.85%</b>	<b>11.55%</b>

### B. Comparison with free-form facial inpainting

In this subsection, we compare our method on CelebA-HQ and FFHQ datasets with state-of-the-art free-form inpainting methods, including Globally&Locally (G&L) [3], Contextual Attention (CA) [40], Partial Convolutions (PConv) [5], Gated Convolution (GConv) [12], Region Normalization (RN) [46], EdgeConnect [13], GMCNN [4], and Co-mod-GAN (CMOD) [9].

1) *Qualitative comparison*: Fig. 5 shows the qualitative comparison of our method with state-of-the-art free-form inpainting methods. All the comparison methods perform well in most cases. G&L [3] tends to produce blurry inpainting while PConv [5] and GConv [12] fail to inpaint large-scale missing regions. Our method and CMOD [9] can generate competitive inpainted results. However, the inpainting of facial attributes cannot be controlled with CMOD [9]. In comparison, with the help of exemplar facial attributes, the inpainting of facial attributes with our EXE-GAN can be controlled diversely.

2) *Quantitative comparison*: Table I and Table II show the quantitative performance comparisons between our methods and others on CelebA-HQ and FFHQ datasets, respectively. Various irregular masks with different masked ratios as well as a fixed rectangle center mask with the size of  $128 \times 128$  were employed to simulate various situations for facial image inpainting. Quantitative results show that our method performs better than most of the compared free-form inpainting methods even though the inpainting of our method is guided by exemplars. Moreover, our EXE-GAN can achieve comparable performance to CMOD [9] with various kinds of masks in terms of FID, U-IDS, and P-IDS.

### C. Comparison with guidance-based facial inpainting

In this subsection, we compare our method on the CelebA-HQ dataset with state-of-the-art guidance-based facial inpainting methods, including sketch-and-color-based facial inpainting SC-FEGAN [11] and landmark-based face inpainting LaFin [10].

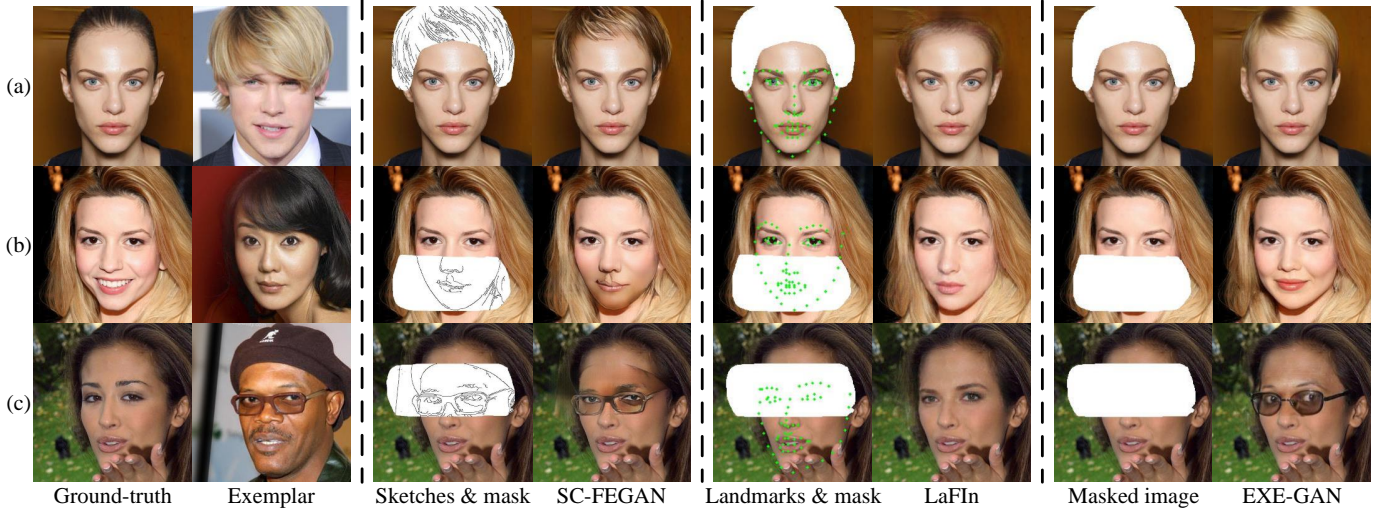


Fig. 6. Qualitative comparison of our method with state-of-the-art guidance-based facial inpainting methods on the CelebA-HQ dataset.

TABLE III  
QUANTITATIVE COMPARISON OF OUR METHOD WITH STATE-OF-THE-ART GUIDANCE-BASED FACIAL INPAINTING METHODS ON THE CELEBA-HQ DATAEST.  $\downarrow$  LOWER IS BETTER.

Metric	Mask	SC-FEGAN [11]	LaFIn [10]	Ours
FID $\downarrow$	10-20%	8.417	5.835	<b>5.074</b>
	20-30%	13.74	9.271	<b>7.946</b>
	30-40%	19.68	12.92	<b>11.04</b>
	40-50%	25.64	16.30	<b>14.03</b>
	50-60%	40.84	21.51	<b>18.19</b>
	Fixed	32.61	10.92	<b>9.414</b>

1) *Experiment settings*: The officially released pre-trained SC-FEGAN and LaFIn models were used in this experiment. SC-FEGAN [11] uses sketches and color as the guidance to generate missing pixels. Therefore, we leveraged the Canny edge detector to automatically generate sketches from the exemplar image. To avoid inconsistency of color in inpainted pixels, we did not introduce color information of the exemplar into missing regions. LaFIn [10] relies on landmarks to fill missing regions. Therefore, we utilized the face alignment network FAN [76] to generate landmarks for the exemplar image. To avoid the misalignment between the guidance information (i.e., sketches and landmarks) and unmasked regions in the masked image, we first extracted the angles of roll, pitch, and yaw from the CelebAMask-HQ dataset [14] and then selected 550 pairs with the similar pose from the testing set. For each pair, we alternately took one facial image as the exemplar and the other one as the masked image to perform facial attribute inpainting. As a consequence, for each kind of masks, we obtained 1100 inpainted images for comparison.

2) *Qualitative comparison*: Fig. 6 shows the qualitative comparison of our method with SC-FEGAN [11] and LaFIn [10]. SC-FEGAN [11] effectively generates facial attributes with shapes guided by sketches but requires more information for high-quality facial attributes inpainting. There may be visual artifacts in the inpainted images, as shown in Fig. 6 (b and c). LaFIn [10] generates facial expressions

similar to exemplars but may fail to inpaint the decorative attributes, such as glasses and hairstyles in Fig. 6 (a and c). In comparison, our method learns the style of facial attributes from the exemplar and can automatically generate exemplar-like facial attributes including decorative attributes. As shown in Fig. 6 (rightmost), our EXE-GAN is able to produce more realistic facial inpainted results with facial attributes similar to exemplars.

3) *Quantitative comparison*: Table III shows the quantitative comparison of our EXE-GAN with SC-FEGAN [11] and LaFIn [10]. FID scores with various mask ratios were compared. Experimental results show that our EXE-GAN is able to achieve the lowest FID scores for all kinds of masks. Our method outperforms the compared methods in terms of the realism for inpainted images guided by exemplars.

4) *User study*: We further conducted a user study to evaluate the effectiveness of our method comprehensively. We randomly selected 100 pairs of images from the 550 pairs mentioned above. Then we randomly divided these pairs into 5 groups and each group consists of 20 pairs with different kinds of inpainting masks. For each pair, we set one image as a masked input and the other as an exemplar to generate inpainting results using the methods of SC-FEGAN [11], LaFIn [10], and our EXE-GAN, respectively. We then randomly distributed one of these groups to a user. For each question, an exemplar image and corresponding three inpainting images of SC-FEGAN [11], LaFIn [10] and our EXE-GAN were provided, users were asked to select the best image based on the visual quality of inpainting and the perceptual similarity to the exemplar. We recruited 63 volunteers to conduct the user survey. The results show that our EXE-GAN (59.67%) obtains the majority of votes compared with SC-FEGAN [11] (12.87%) and LaFIn [10] (27.46%). The user study validates that our EXE-GAN performs better than the compared methods in the exemplar-guided facial inpainting.



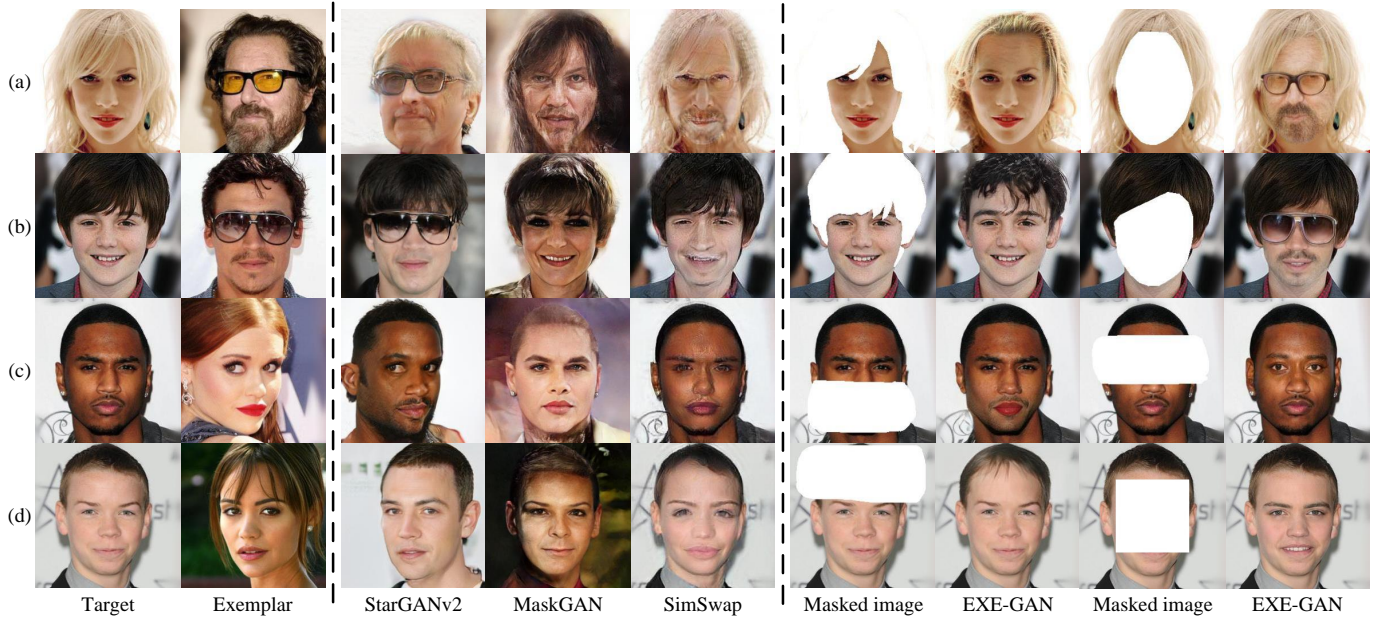


Fig. 7. Qualitative comparison of our method with state-of-the-art facial attribute transfer methods on the CelebA-HQ dataset.

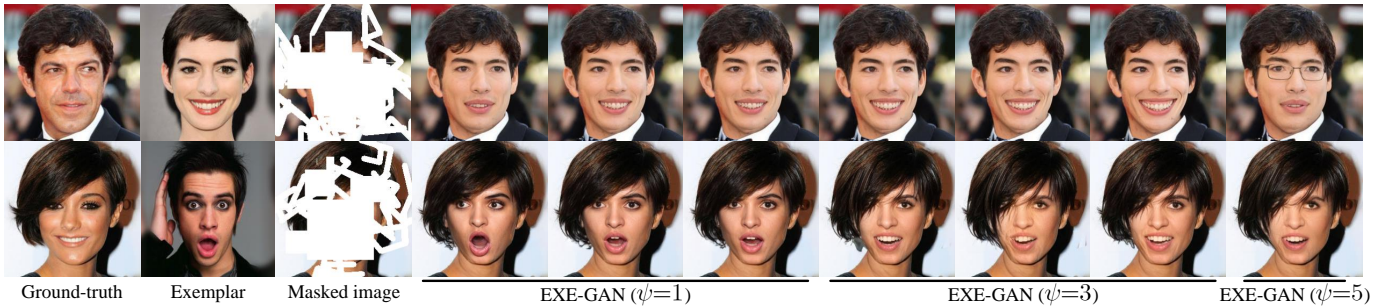


Fig. 8. Examples of diverse facial inpainting with the inherent stochasticity of EXE-GAN. The parameter  $\psi$  denotes the style scale. These results show that our method can inherently produce diverse results without affecting the exemplar facial attributes of inpainted images. Please zoom-in for more details.

#### D. Comparison with facial attribute transfer

In this subsection, we compare our method on the CelebA-HQ dataset with state-of-the-art facial attribute transfer methods, including StarGANv2 [17], MaskGAN [14], and SimSwap [54].

1) *Experiment settings*: The pre-trained models of StarGANv2 [17], MaskGAN [14], and SimSwap [54] provided in the official website repository were used in this experiment. For StarGANv2 [17], we set the target image as the “reference” image and the exemplar image as the “source” image. For MaskGAN [14], we extracted semantic masks of target images from the CelebAMask-HQ dataset [14] and obtained the style copied results based on semantic masks and exemplars. SimSwap [54] directly performs the exemplar-guided face synthesis with the target and exemplar images. Our EXE-GAN synthesizes facial attributes for masked regions of target images guided by exemplar images.

2) *Qualitative comparison*: Fig. 7 shows the qualitative comparison of our method with state-of-the-art facial transfer

methods. StarGANv2 [17] can transform a target image reflecting the identity of exemplar. However, it leaves users little freedom to manipulate face images interactively. MaskGAN [17] transfers the style of exemplar to the target face using the semantic mask. It requires to project images into semantic masks and then to reconstruct images from the mask manifold. As a result, it may introduce irrelevant changes for fine details in the background. SimSwap [54] can transfer the identity of a source face to a target face and preserve facial attributes of the target. Nevertheless, it does not allow users to flexibly select regions for face editing. In comparison, our method does not change any pixel for known regions and allows users much freedom to perform the facial attribute manipulation interactively. Our EXE-GAN produces visually realistic results with facial attributes of exemplars, including gender, makeup style, hairstyle, decorative style (e.g., wearing eyeglasses).

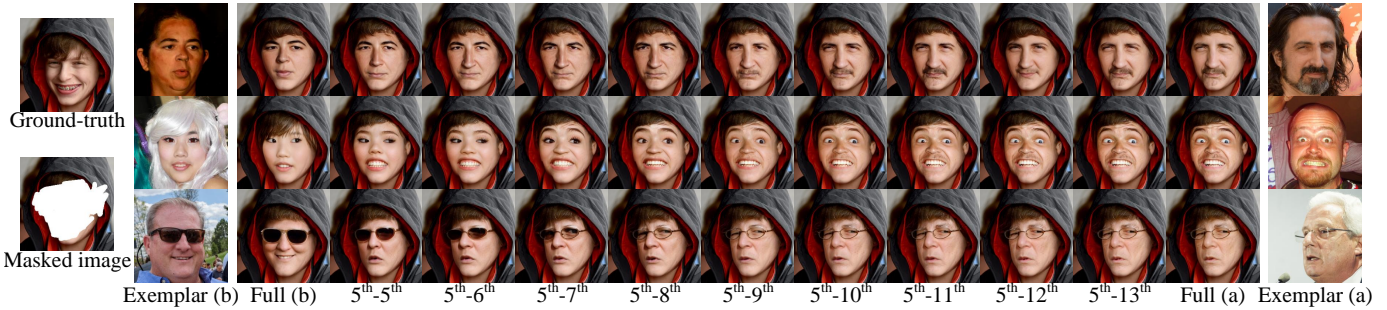


Fig. 9. Examples of style mixing-based diverse inpainting of EXE-GAN. In each example, values of  $i^{th}$ - $j^{th}$  channels of style code of exemplar b are replaced by those of exemplar a. Please zoom-in for more details.

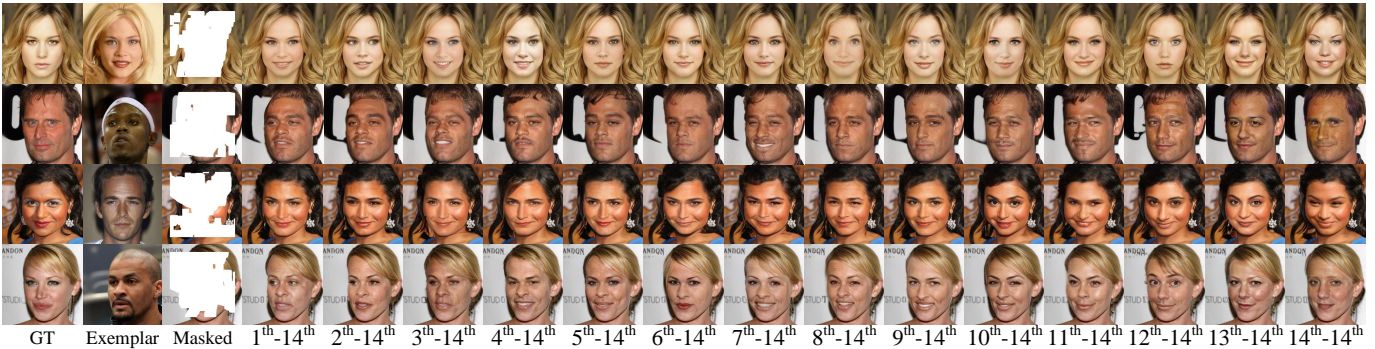


Fig. 10. Examples of code-tuning diverse inpainting of EXE-GAN. In each example, values of  $i^{th}$ - $j^{th}$  channels of  $\phi \in \mathbb{R}^{18 \times 1}$  are set as 1 and remaining values are set as 0. Please zoom-in for more details.

### E. Discussion on diverse facial inpainting

In this subsection, we demonstrate that our method can perform high-quality diverse facial inpainting in the following four aspects: the inherent stochasticity, multiple exemplar-based diverse inpainting, style mixing-based diverse inpainting, and code-tuning diverse inpainting.

1) *The inherent stochasticity*: By adding per-pixel noise after each convolution layer [23], [58] and leveraging the injected stochastic style representations [9], our method can produce diverse inpainting results, even when the masked input and exemplar are fixed. In addition, we can apply the truncation trick to amplify the stochastic styles by tuning the style scale  $\psi$  as in [23], [58]. The amplified stochastic style codes are modulated into corresponding style layers with values of 0 in the binary vector  $\phi$  in Eq.1. Diverse inpainting results with the inherent stochasticity are as shown in Fig. 8.

2) *Multiple exemplar-based diverse inpainting*: Since our EXE-GAN helps the generator learn the mapping between injected exemplar representations and corresponding facial attributes, our method can produce diverse inpainting results guided by multiple exemplars. As shown in Fig. 1, for a masked input, our EXE-GAN produces diverse high-quality inpainting results by leveraging multiple exemplar facial attributes.

3) *Style mixing-based diverse inpainting*: Our EXE-GAN can generate diverse inpainting results by mixing two exemplar style latent codes. We first employ the style encoder  $E$  to ob-

tain two exemplar style codes  $w_a$  and  $w_b$  from two exemplars  $a$  and  $b$ , respectively. Then, we apply the style mixing [23], [58] on the two latent codes, where  $w_a$  applies before the crossover point and  $w_b$  after it. By simply changing the crossover point, we can obtain multiple mixed latent codes. Fig. 9 shows examples of style mixing-based diverse inpainting. We obtain 10 extra inpainting results by moving the crossover point from  $5^{th}$  to  $14^{th}$  indexes in the vector  $\phi$ .

4) *Code-tuning diverse inpainting*: The binary vector  $\phi$  is the hyperparameter for tuning which kind of style (stochastic or exemplar) codes are modulated into the generator. We can generate diverse inpainting results with different settings of  $\phi$ . As shown in Fig. 10, we can tune the degree of exemplar facial attributes with various settings of  $\phi$ . From the figure we can find that the more exemplar style codes are modulated the more exemplar facial attributes will present in the inpainted images.

We have demonstrated diverse facial inpainting using the inherent stochasticity, multiple exemplars, style mixing, and code tuning. Note that these four aspects of diverse facial inpainting can be combined together to achieve even diverse facial inpainting.

### F. Ablation study

1) *Ablation study on Co-mod-GAN*: To demonstrate the effectiveness of the proposed spatial variant gradient layer, we experimented to apply our SVGL to Co-mod-GAN [9] for the

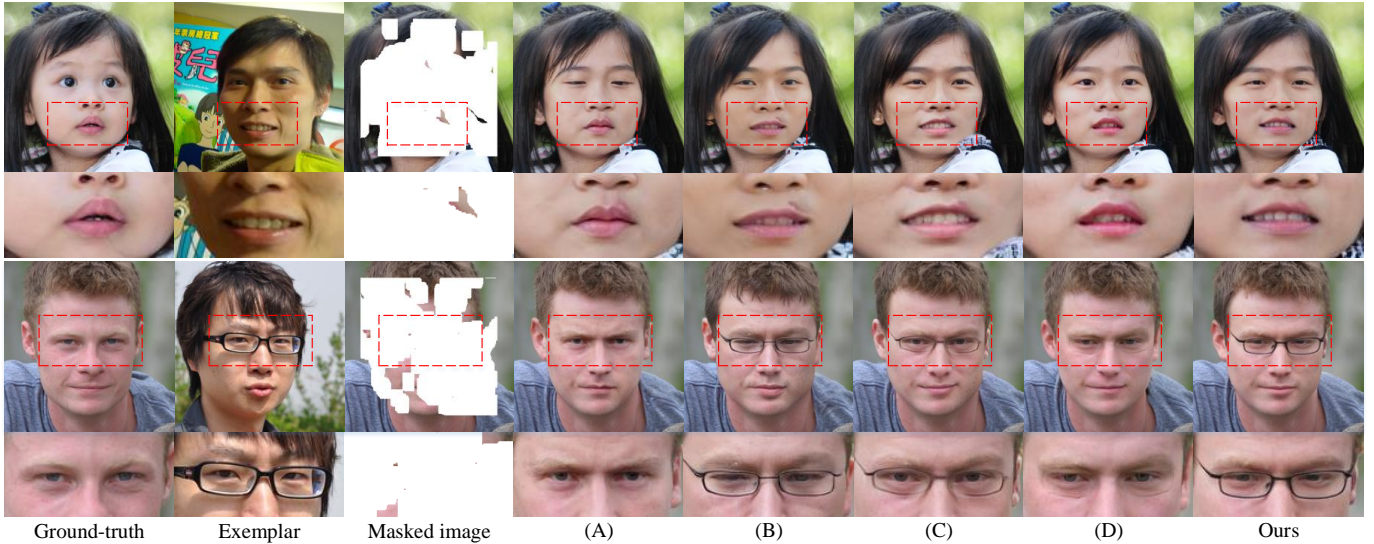


Fig. 11. Qualitative examples of the ablation study for large-scale facial inpainting by exemplars with (A) removing SVGL-based  $\mathcal{L}_{attr}$  in EXE-GAN, (B) removing SVGL-based  $\mathcal{L}_{lips}$  in EXE-GAN, (C) replacing SVGL-based  $\mathcal{L}_{attr}$  with standard  $\mathcal{L}_{attr}$  in EXE-GAN, (D) replacing SVGL-based  $\mathcal{L}_{lips}$  with standard  $\mathcal{L}_{lips}$  in EXE-GAN, and (Ours) EXE-GAN. Please zoom in for more details.

TABLE IV

ABLATION STUDY FOR LARGE-SCALE FACIAL INPAINTING WITH (A) BASELINE CO-MOD-GAN [9], (B) CO-MOD-GAN + STANDARD  $\mathcal{L}_{lips}$ , AND (C) CO-MOD-GAN + SVGL-BASED  $\mathcal{L}_{lips}$ . RESULTS ARE AVERAGED OVER 5 RUNS. **BOLD**: TOP-2 QUANTITY.

Method	CelebA-HQ			FFHQ		
	FID↓	U-IDS↑	P-IDS↑	FID↓	U-IDS↑	P-IDS↑
A	9.733	9.68%	4.00%	4.000	26.19%	12.88%
B	<b>8.993</b>	<b>10.87%</b>	<b>4.70%</b>	<b>3.432</b>	<b>29.08%</b>	<b>13.52%</b>
C	<b>8.985</b>	<b>11.25%</b>	<b>4.85%</b>	<b>3.318</b>	<b>29.97%</b>	<b>14.88%</b>

image inpainting task. The quantitative ablation study results are shown in Table IV. As shown in Table IV, the performance is improved by adding the LPIPS loss into the baseline Co-mod-GAN. The quantitative scores are considerably improved by further introducing SVGL in the LPIPS loss for Co-mod-GAN. The SVGL-based LPIPS loss helps the generator focus more on pixels close to the hole boundary to avoid visual inconsistency and still encourage inherent stochasticity with less constraints to pixels away from the boundary. This ablation study shows that the proposed SVGL can effectively boost the performance of image inpainting.

2) *Ablation study on EXE-GAN*: We further investigated the effectiveness of each component in this paper by performing the ablation study on the proposed EXE-GAN framework. The quantitative results are shown in Table V. We also present qualitative examples in Fig. 11 to better express visual effects. When removing the SVGL-based attribute loss in EXE-GAN (A), it lowers the visual similarity of facial attributes between the generated and exemplar with comparable quantitative scores. When removing the SVGL-based LPIPS loss (B), both the quantitative measures and visual qualities drop dramatically. When replacing the SVGL-based attribute loss with the standard attribute loss (C), SVGL is not employed for the attribute loss. There may be visible boundary inconsistencies

TABLE V

ABLATION STUDY FOR LARGE-SCALE FACIAL INPAINTING BY EXEMPLARS WITH (A) REMOVING SVGL-BASED  $\mathcal{L}_{attr}$  IN EXE-GAN, (B) REMOVING SVGL-BASED  $\mathcal{L}_{lips}$  IN EXE-GAN, (C) REPLACING SVGL-BASED  $\mathcal{L}_{attr}$  WITH STANDARD  $\mathcal{L}_{attr}$  IN EXE-GAN, (D) REPLACING SVGL-BASED  $\mathcal{L}_{lips}$  WITH STANDARD  $\mathcal{L}_{lips}$  IN EXE-GAN, AND (OURS) EXE-GAN. RESULTS ARE AVERAGED OVER 5 RUNS. **BOLD**: TOP-2 QUANTITY.

Method	CelebA-HQ			FFHQ		
	FID↓	U-IDS↑	P-IDS↑	FID↓	U-IDS↑	P-IDS↑
A	<b>9.714</b>	<b>11.38%</b>	<b>4.65%</b>	4.453	23.84%	9.86%
B	10.207	7.37%	2.95%	4.726	23.50%	9.53%
C	10.433	8.875%	3.35%	4.909	22.46%	8.75%
D	<b>9.804</b>	8.875%	<b>4.25%</b>	<b>4.408</b>	<b>24.61%</b>	<b>10.04%</b>
Ours	9.967	<b>9.175%</b>	3.85%	<b>4.353</b>	<b>24.33%</b>	<b>9.92%</b>

in the inpainted results and the quantitative performance also degrades to some extent. When replacing the SVGL-based LPIPS loss with the standard LPIPS loss (D), the visual similarities of facial attributes (e.g., facial expression, wearing glasses) between the generated and the exemplar decrease, while the quantitative scores are comparable to EXE-GAN for both testing datasets. In this case, the standard  $\mathcal{L}_{lips}$  is applied to all pixels of images to enforce the generator to reconstruct the contents of ground-truth instead of exemplar attributes, as demonstrated in Fig. 11. In comparison, our EXE-GAN is able to produce visually realistic inpainted facial images with facial attributes similar to exemplars and competitive quantitative scores.

## V. CONCLUSIONS AND FUTURE WORK

In this paper, we have presented a novel diverse facial inpainting framework for realistic facial inpainting by taking advantage of exemplar facial attributes. An attribute similarity metric was introduced to help the generative network learn the style of facial attributes from the exemplar. We further proposed a novel spatial variant gradient backpropagation

technique to address the issue of visual inconsistency on the hole boundary. A number of experimental comparisons and results have demonstrated the effectiveness of the proposed method.

In the future, we would like to further improve the mapping between facial attributes and embedded style codes using more advanced embedding algorithms. In addition, we plan to apply the proposed spatial variant gradient backpropagation to other image editing applications.

## REFERENCES

- [1] Q. Gao, X. Shu, and X. Wu, "Deep restoration of vintage photographs from scanned halftone prints," in *Proc. ICCV*, 2019, pp. 4120-4129.
- [2] X. Wu, L. Li, F. Zhang, J. Liu, J. Wang, A. Shamir, and S. Hu, "Deep portrait image completion and extrapolation," *IEEE Transactions on Image Processing*, vol. 29, pp. 2344-2355, 2020.
- [3] S. Iizuka, E. Simo-Serra, and H. Ishikawa, "Globally and locally consistent image completion," *ACM Transactions on Graphics*, vol. 36, no. 4, pp. 1-14, 2017.
- [4] Y. Wang, X. Tao, X. Qi, Xi. Shen, and J. Jia, "Image inpainting via generative multi-column convolutional neural networks," in *Proc. NeurIPS*, 2018, pp. 331-340.
- [5] G. Liu, F. A. Reda, K. J. Shih, T. C. Wang, A. Tao, and B. Catanzaro, "Image inpainting for irregular holes using partial convolutions," in *Proc. ECCV*, 2018, pp. 85-100.
- [6] Z. Yi, Q. Tang, S. Azizi, D. Jang, and Z. Xu, "Contextual residual aggregation for ultra high-resolution image inpainting," in *Proc. CVPR*, 2020, pp. 7508-7517.
- [7] L. Zhao, Q. Mo, S. Lin, Z. Wang, Z. Zuo, H. Chen, W. Xing, and D. Lu, "UCTGAN: Diverse image inpainting based on unsupervised cross-space translation," in *Proc. CVPR*, 2020, pp. 5741-5750.
- [8] C. Zheng, T. J. Cham, and J. Cai, "Pluralistic image completion," in *Proc. CVPR*, 2019, pp. 1438-1447.
- [9] S. Zhao, J. Cui, Y. Sheng, Y. Dong, X. Liang, E. I. Chang, and Y. Xu, "Large scale image completion via co-modulated generative adversarial networks," in *Proc. ICLR*, 2021.
- [10] Y. Yang and X. Guo, "LaFin: Generative landmark guided face inpainting," in *Proc. PRCV*, 2020, pp. 14-26.
- [11] Y. Jo and J. Park, "SC-FEGAN: Face editing generative adversarial network with user's sketch and color," in *Proc. ICCV*, 2019, pp. 1745-1753.
- [12] J. Yu, Z. Lin, J. Yang, X. Shen, X. Lu, and T. S. Huang, "Free-form image inpainting with gated convolution," in *Proc. ICCV*, 2019, pp. 4471-4480.
- [13] K. Nazeri, E. Ng, T. Joseph, F. Qureshi, and M. Ebrahimi, "EdgeConnect: Generative image inpainting with adversarial edge learning," *arXiv preprint*, arXiv:1901.00212, 2019.
- [14] C. H. Lee, Z. Liu, L. Wu, and P. Luo, "MaskGAN: Towards diverse and interactive facial image manipulation," in *Proc. CVPR*, 2020, pp. 5549-5558.
- [15] A. Chen, R. Liu, L. Xie, Z. Chen, H. Su, and J. Yu, "SofGAN: A portrait image generator with dynamic styling," *ACM transactions on Graphics*, vol. 41, no. 1, pp. 1-26, 2021.
- [16] Y. Choi, M. Choi, M. Kim, J. W. Ha, S. Kim, and J. Choo, "StarGAN: Unified generative adversarial networks for multi-domain image-to-image translation," in *Proc. CVPR*, 2018, pp. 8789-8797.
- [17] Y. Choi, Y. Uh, J. Yoo, and J. W. Ha, "StarGAN v2: Diverse image synthesis for multiple domains," in *Proc. CVPR*, 2020, pp. 8188-8197.
- [18] T. Xiao, J. Hong, and J. Ma, "ELEGANT: Exchanging latent encodings with GAN for transferring multiple face attributes," in *Proc. ECCV*, 2018, pp. 168-184.
- [19] X. Li, S. Zhang, J. Hu, L. Cao, X. Hong, X. Mao, F. Huang, Y. Wu, and R. Ji, "Image-to-image translation via hierarchical style disentanglement," in *Proc. CVPR*, 2021, pp. 8639-8648.
- [20] Y. Wu, Y. L. Yang, Q. Xiao, and X. Jin, "Coarse-to-fine: Facial structure editing of portrait images via latent space classifications," *ACM Transactions on Graphics*, vol. 40, no. 4, pp. 1-13, 2021.
- [21] R. Zhang, P. Isola, A. A. Efros, E. Shechtman, and O. Wang, "The unreasonable effectiveness of deep features as a perceptual metric," in *Proc. CVPR*, 2018, pp. 586-595.
- [22] T. Karras, T. Aila, S. Laine, and J. Lehtinen, "Progressive growing of GANs for improved quality, stability, and variation," *arXiv preprint*, arXiv:1710.10196, 2017.
- [23] T. Karras, S. Laine, and T. Aila, "A style-based generator architecture for generative adversarial networks," in *Proc. CVPR*, 2019, pp. 4401-4410.
- [24] C. Ballester, M. Bertalmio, V. Caselles, G. Sapiro, and J. Verdera, "Filling-in by joint interpolation of vector fields and gray levels," *IEEE Transactions on Image Processing*, vol. 10, no. 8, pp. 1200-1211, 2001.
- [25] M. Bertalmio, G. Sapiro, V. Caselles, and C. Ballester, "Image inpainting," in *Proc. SIGGRAPH*, 2000, pp. 417-424.
- [26] A. Levin, A. Zomet, and Y. Weiss, "Learning how to inpaint from global image statistics," in *Proc. ICCV*, 2003, pp. 305-312.
- [27] A. A. Efros and W. T. Freeman, "Image quilting for texture synthesis and transfer," in *Proc. SIGGRAPH*, 2001, pp. 341-346.
- [28] A. Telea, "An image inpainting technique based on the fast marching method," *Journal of Graphics Tools*, vol. 9, no. 1, pp. 23-34, 2004.
- [29] V. Kwatra, I. Essa, A. Bobick, and N. Kwatra, "Texture optimization for example-based synthesis," *ACM Transactions on Graphics*, vol. 24, no. 3, pp. 795-802, 2005.
- [30] C. Barnes, E. Shechtman, A. Finkelstein, and D. B. Goldman, "Patch-Match: A randomized correspondence algorithm for structural image editing," *ACM Transactions on Graphics*, vol. 28, no. 3, pp. 24:1-24:11, 2009.
- [31] H. Zhao, H. Guo, X. Jin, J. Shen, X. Mao, and J. Liu, "Parallel and efficient approximate nearest patch matching for image editing applications," *Neurocomputing*, vol. 305, pp. 39-50, 2018.
- [32] D. Simakov, Y. Caspi, E. Shechtman, and M. Irani, "Summarizing visual data using bidirectional similarity," in *Proc. CVPR*, 2008, pp. 1-8.
- [33] D. Ding, S. Ram, and J. J. Rodríguez, "Image inpainting using nonlocal texture matching and nonlinear filtering," *IEEE Transactions on Image Processing*, vol. 28, no. 4, pp. 1705-1719, 2019.
- [34] I. Goodfellow, J. Pouget-Abadie, M. Mirza, B. Xu, D. Warde-Farley, S. Ozair, A. Courville, and Y. Bengio, "Generative adversarial nets," in *Proc. NIPS*, 2014.
- [35] R. Köhler, C. Schuler, B. Schölkopf, and S. Harmeling, "Mask-specific inpainting with deep neural networks," in *Proc. German Conference on Pattern Recognition*, 2014, pp. 523-534.
- [36] J. S. Ren, L. Xu, Q. Yan, and W. Sun, "Shepard convolutional neural networks," in *Proc. NIPS*, 2015, pp. 901-909.
- [37] J. Xie, L. Xu, and E. Chen, "Image denoising and inpainting with deep neural networks," in *Proc. NIPS*, 2012, pp. 341-349.
- [38] D. Pathak, P. Krahenbuhl, J. Donahue, T. Darrell, and A. A. Efros, "Context encoders: Feature learning by inpainting," in *Proc. CVPR*, 2016, pp. 2536-2544.
- [39] H. Liu, B. Jiang, Y. Xiao, and C. Yang, "Coherent semantic attention for image inpainting," in *Proc. ICCV*, 2019, pp. 4169-4178.
- [40] J. Yu, Z. Lin, J. Yang, X. Shen, X. Lu, and T. S. Huang, "Generative image inpainting with contextual attention," in *Proc. CVPR*, 2018, pp. 5505-5514.
- [41] C. Xie, S. Liu, C. Li, M. M. Cheng, W. Zuo, X. Liu, S. Wen, and E. Ding, "Image inpainting with learnable bidirectional attention maps," in *Proc. ICCV*, 2019, pp. 8858-8867.
- [42] Z. Yan, X. Li, M. Li, W. Zuo, and S. Shan, "Shift-net: Image inpainting via deep feature rearrangement," in *Proc. ECCV*, 2018, pp. 1-17.
- [43] A. Lahiri, A. K. Jain, S. Agrawal, P. Mitra, and P. K. Biswas, "Prior guided GAN based semantic inpainting," in *Proc. CVPR*, 2020, pp. 13696-13705.
- [44] M. C. Sagong, Y. G. Shin, S. W. Kim, S. Park, and S. J. Ko, "PEPSI: Fast image inpainting with parallel decoding network," in *Proc. CVPR*, 2019, pp. 11360-11368.
- [45] J. Li, N. Wang, L. Zhang, B. Du, and D. Tao, "Recurrent feature reasoning for image inpainting," in *Proc. CVPR*, 2020, pp. 7760-7768.
- [46] T. Yu, Z. Guo, X. Jin, S. Wu, Z. Chen, W. Li, Z. Zhang, and S. Liu, "Region normalization for image inpainting," in *Proc. AAAI*, vol. 34, no. 07, 2020, pp. 12733-12740.
- [47] C. Yang, X. Lu, Z. Lin, E. Shechtman, O. Wang, and H. Li, "High-resolution image inpainting using multi-scale neural patch synthesis," in *Proc. CVPR*, 2017, pp. 6721-6729.
- [48] Y. Zeng, J. Fu, H. Chao, and B. Guo, "Learning pyramid-context encoder network for high-quality image inpainting," in *Proc. CVPR*, 2019, pp. 1486-1494.
- [49] T. Wang, H. Ouyang, and Q. Chen, "Image inpainting with external-internal learning and monochromatic bottleneck," in *Proc. CVPR*, 2021, pp. 5120-5129.
- [50] Y. Ren, X. Yu, R. Zhang, T. H. Li, S. Liu, and G. Li, "Structureflow: Image inpainting via structure-aware appearance flow," in *Proc. ICCV*, 2019, pp. 181-190.
- [51] W. Xiong, J. Yu, Z. Lin, J. Yang, X. Lu, C. Barnes, and J. Luo, "Foreground-aware image inpainting," in *Proc. CVPR*, 2019, pp. 5840-5848.

- [52] J. Guo, Z. Qian, Z. Zhou, and Y. Liu, "MulGAN: Facial attribute editing by exemplar," *arXiv preprint*, arXiv:1912.12396, 2019.
- [53] L. Li, J. Bao, H. Yang, D. Chen, and F. Wen, "FaceShifter: Towards high fidelity and occlusion aware face swapping," in *Proc. CVPR*, 2020, pp. 5074-5083.
- [54] R. Chen, X. Chen, B. Ni, and Y. Ge, "SimSwap: An efficient framework for high fidelity face swapping," in *Proc. ACM MM*, 2020, pp. 2003-2011.
- [55] G. Perarnau, J. V. D. Weijer, B. Raducanu, and J. M. Álvarez, "Invertible conditional GANs for image editing," *arXiv preprint*, arXiv:1611.06355, 2016.
- [56] G. Lample, N. Zeghidour, N. Usunier, A. Bordes, L. Denoyer, and M. A. Ranzato, "Fader networks: Manipulating images by sliding attributes," in *Proc. NIPS*, 2017.
- [57] P. Zhu, R. Abdal, Y. Qin, and P. Wonka, "SEAN: Image synthesis with semantic region-adaptive normalization," in *Proc. CVPR*, 2020, pp. 5103-5112.
- [58] T. Karras, S. Laine, M. Aittala, J. Hellsten, J. Lehtinen, and T. Aila, "Analyzing and improving the image quality of styleGAN," in *Proc. CVPR*, 2020, pp. 8110-8119.
- [59] R. Abdal, Y. Qin, and P. Wonka, "Image2styleGAN: How to embed images into the styleGAN latent space?" in *Proc. CVPR*, 2019, pp. 4432-4441.
- [60] R. Abdal, Y. Qin, and P. Wonka, "Image2styleGAN++: How to edit the embedded images?" in *Proc. CVPR*, 2020, pp. 8296-8305.
- [61] J. Y. Zhu, P. Krähenbühl, E. Shechtman, and A. A. Efros, "Generative visual manipulation on the natural image manifold," in *Proc. ECCV*, 2016, pp. 597-613.
- [62] E. Richardson, Y. Alaluf, O. Patashnik, Y. Nitzan, Y. Azar, S. Shapiro, and D. Cohen-Or, "Encoding in style: a styleGAN encoder for image-to-image translation," in *Proc. CVPR*, 2021, pp. 2287-2296.
- [63] O. Tov, Y. Alaluf, Y. Nitzan, O. Patashnik, and D. Cohen-Or, "Designing an encoder for styleGAN image manipulation," *ACM Transactions on Graphics*, vol. 40, no. 4, pp. 1-14, 2021.
- [64] J. Zhu, Y. Shen, D. Zhao, and B. Zhou, "In-domain GAN inversion for real image editing," in *Proc. ECCV*, 2020, pp. 592-608.
- [65] L. Mescheder, A. Geiger, and S. Nowozin, "Which training methods for GANs do actually converge?" in *Proc. ICML*, 2018.
- [66] J. Deng, J. Guo, N. Xue, and S. Zafeiriou, "ArcFace: Additive angular margin loss for deep face recognition," in *Proc. CVPR*, 2019, pp. 4690-4699.
- [67] B. Liu, Y. Zhu, K. Song, and A. Elgammal, "Towards faster and stabilized GAN training for high-fidelity few-shot image synthesis," in *Proc. ICLR*, 2020.
- [68] J. Johnson, A. Alahi, and F. F. Li, "Perceptual losses for real-time style transfer and super-resolution," in *Proc. ECCV*, 2016, pp. 694-711.
- [69] S. Guan, Y. Tai, B. Ni, F. Zhu, F. Huang, and X. Yang, "Collaborative learning for faster styleGAN embedding," *arXiv preprint*, arXiv:2007.01758, 2020.
- [70] K. Simonyan and A. Zisserman, "Very deep convolutional networks for large-scale image recognition," *arXiv preprint*, arXiv:1409.1556, 2014.
- [71] L. A. Gatys, A. S. Ecker, and M. Bethge, "Image style transfer using convolutional neural networks," in *Proc. CVPR*, 2016, pp. 2414-2423.
- [72] Y. Ganin and V. Lempitsky, "Unsupervised domain adaptation by backpropagation," in *Proc. PMLR*, 2015, pp. 1180-1189.
- [73] X. Sun, X. Ren, S. Ma, and H. Wang, "meProp: Sparsified back propagation for accelerated deep learning with reduced overfitting," in *Proc. PMLR*, 2017, pp. 3299-3308.
- [74] Z. Liu, P. Luo, X. Wang, and X. Tang, "Deep learning face attributes in the wild," in *Proc. ICCV*, 2015.
- [75] M. Heusel, H. Ramsauer, T. Unterthiner, B. Nessler, and S. Hochreiter, "GANs trained by a two time-scale update rule converge to a local nash equilibrium," in *Proc. NIPS*, 2017, pp. 6626-6637.
- [76] A. Bulat and G. Tzimiropoulos, "How far are we from solving the 2d & 3d face alignment problem? (and a dataset of 230,000 3d facial landmarks)," in *Proc. ICCV*, 2017, pp. 1021-1030.